Academic Journal of Engineering and Technology Science
ISSN 2616-5767 Vol.9, Issue 3: 41-50, DOI: 10.25236/AJETS.2026.090306

Micro-Motion Characteristic Analysis of Precision Linear Motion Platform Based on Component-Refined Modeling

Yan Tan*, Hao Tang

Hunan Provincial Key Laboratory of Health Maintenance for Mechanical Equipment, Hunan University of Science and Technology, Xiangtan, China
**Corresponding Author*

Abstract: *The dynamic model of a precision linear motion platform serves as the foundation for achieving high-quality motion at micro-stroke scales. The three fundamental elements of system motion are displacement, velocity, and acceleration. High-quality motion is ultimately reflected in displacement accuracy, while velocity and acceleration indirectly influence displacement precision. Therefore, this paper proposes a component-refined dynamic modeling method aimed at analyzing the variation patterns of velocity at micro-stroke scales. First, along the motion transmission path, motion types are distinguished, transmission modes are analyzed, and a qualitative dynamic modeling framework is established. Second, refined equivalent models of the input source and the motion conversion mechanism are developed respectively, and the coupling mechanism between them is constructed. Finally, the simulated velocity curves are compared with experimental velocity curves at stroke scales of 10 μm, 20 μm, 50 μm, and 100 μm. The method provides a certain degree of prediction of velocity magnitude, as well as the local peaks, troughs, and convergence trends of the velocity curves, thereby validating the effectiveness of the dynamic model.*

Keywords: *Component-refined, dynamic model, Precision linear motion platform, Micro-motion characteristic analysis*

1. Introduction

Precision linear motion platforms are widely employed in fields such as optical device fabrication and multi-axis robotics, enabling high-precision positioning and performing critical core tasks, thereby playing a crucial role in the overall operational performance of the system. Positioning error serves as a key parameter for evaluating the motion accuracy of precision linear motion platforms and largely determines the assessment of positioning precision. Positioning accuracy is not only an important metric within standard accuracy systems but also closely correlates with system operational performance. Therefore, analyzing motion characteristics across different scales is of great significance for enhancing the motion accuracy of precision linear motion platforms.

The three fundamental elements of system motion are displacement, velocity, and acceleration. Among them, displacement serves as the direct manifestation of error, while velocity and acceleration are often taken as control entry points that indirectly affect displacement and error. Aguada[1]discussed an improved kinematic model for machine tools and applied it to the study of error sources in uncertainty analysis. Du[2]established a geometric error model for single-axis assembly based on Jacobian–Torsor theory, enabling the identification of key error sources in single-axis assembly. Huang[3]developed a geometric error model for three-axis machine tools using homogeneous transformation matrices combined with the Abbe principle and Bryan principle. The aforementioned studies focus on the transmission of motion displacement and the resulting geometric error deviations. To further improve displacement accuracy, indirect influences must be considered, requiring further analysis in conjunction with system dynamic parameters.

Qian[4]addressed the influence of vibration by considering the correlation between motion position and system dynamic characteristics. They established a dynamic equation based on the Ritz series method and analyzed the axial and torsional vibrations at different positions, distinguishing the vibration variations caused by position changes. Wu[5]introduced the variation in distance between the ram centroid and the oil film support center during guideway operation to establish an improved dynamic model for accurately predicting the motion of ram-type guideways. The model demonstrated that motion errors are significantly affected by dynamic effects. Tang[6]investigated the repeated positioning accuracy of precision linear motion platforms by establishing a mapping relationship between dynamic parameters and repeated positioning accuracy based on micro-motion characteristics. Huang[7]developed a linear parameter-varying dynamic model for high-quality and high-efficiency control of servo ball screw transmission systems, considering the effects of position and load on dynamic characteristics. Zhao[8]proposed a load distribution model under combined loads that accounts for ball geometric errors, starting from the differences in ball contact states within ball screws, thereby enabling position accuracy prediction of ball screw pairs. Zha[9]established a guideway profile error function and identified the initial oil film gap and throttle ratio as the main factors affecting motion errors. Ohta[10]developed an elastic deformation model for rolling guideways considering the elastic deformation of both the guideway and rolling elements. Khim[11]constructed a transfer function relationship between guideway geometric errors and restoring forces, and further established equilibrium equations during motion to analyze the five-degree-of-freedom motion errors of guideways. It can be seen that incorporating dynamic characteristic analysis can enhance the alignment between practical applications and theoretical calculations, thereby improving the mathematical model of motion systems. However, the aforementioned studies lack sufficient depth in integrating geometric errors with drive system characteristics, particularly in the context of micro-strokes where further analysis of upstream influences in the motion transmission chain is needed. This limitation results in insufficient alignment between mathematical models and practical conditions at this scale.

In summary, research on motion characteristics at the micro-stroke scale still faces the following issues that require urgent resolution: the coupling mechanism of the motion chain and the equivalent modeling of individual components. This study focuses on the velocity characteristics of precision linear motion platforms and conducts an in-depth analysis using component-equivalent dynamic models. By analyzing the motion characteristics of the drive motor and examining the constraining effects of geometric errors in the moving components, an equivalent model of the ball screw is jointly constructed to enable accurate description of motion characteristics at the micro-stroke scale. Corresponding measurement experiments are designed to validate the effectiveness of the dynamic model, providing a theoretical basis for subsequent high-efficiency control and improvement of motion displacement accuracy.

2. Structure and dynamic modeling of the motion platform

2.1. Structure of the precision linear motion platform

From the perspective of the core motion transmission chain, micro-scale high-precision linear motion platforms mainly include the following structures: screw-guide type, linear motor direct drive type, etc. Considering cost control, high applicability, and high precision, a roller screw-guide type micro-scale precision linear motion platform driven by a high-resolution stepper motor is widely used in the market. The mechanical structure model of the motion platform is shown in Figure 1.

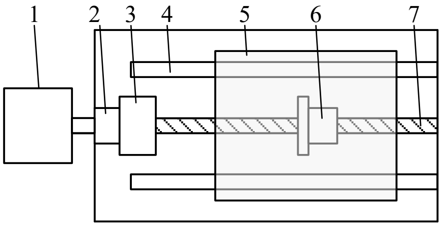

1. Motor
2. Coupling
3. Bearing housing and bearings
4. Guideway
5. worktable
6.Nut
7.Screw

Figure 1: Structure of the precision linear motion platform.

From the figure above, the core components of the platform motion transmission chain can be identified: the motor shaft, coupling, lead screw shaft, and nut (worktable). During motion transmission, the stepper motor inputs an angular displacement, which drives the lead screw shaft to rotate by a certain angle via the coupling. Under the principle of screw transmission, the balls act as contact elements to propel the nut (worktable). In this process, motion displacement errors originate from two aspects. On one hand, geometric errors are associated with manufacturing imperfections. On the other hand, dynamic responses—such as inconsistencies in the steady-state position of the motor due to nonlinear factors and random disturbances—also contribute to error. The ball screw system inherently exhibits both types of errors, resulting in certain inconsistencies between measured error curves. This objectively leads to superimposed constraints from geometric errors and random error distributions. To establish a comprehensive mathematical model that accurately describes motion characteristics, the transmission system is expanded along the axis system, and refined equivalent models are developed for each component.

2.2. Equivalent models of motion chain components

As shown in Figure 2, the relative positions of the rotor teeth and stator teeth of the stepper motor are illustrated. According to the numbered sequence in the figure, the relative positions of the teeth correspond to four states: aligned, offset by 1/4 tooth pitch, offset by 1/2 tooth pitch, and offset by 3/4 tooth pitch (equivalent to an offset of 1/4 tooth pitch).

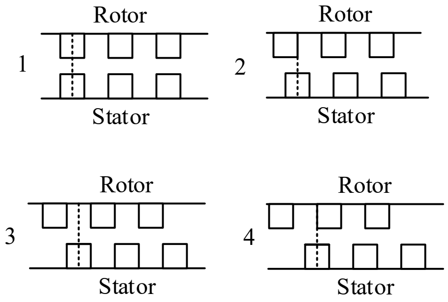

Figure 2: Relative position between rotor teeth and stator teeth.

When power is applied but no pulse is given, the system remains in the aligned state. Upon receiving a pulse, the stator in State 2 generates a magnetomotive force, attracting the rotor teeth to align in order to minimize reluctance, thereby producing an electromagnetic torque. This electromagnetic torque can be equivalent to a nonlinear spring, which aligns the rotor with the stator in State 2. The motor shaft is then connected to the lead screw shaft via a coupling, forming a complete shaft system. Figure 3 shows the equivalent model of the shaft system.

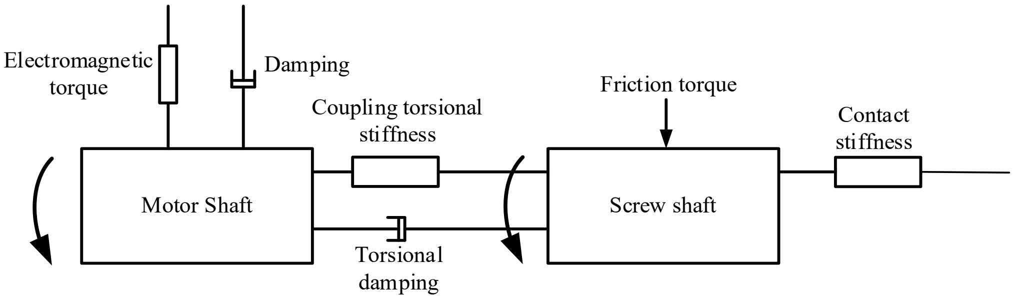

Figure 3: Equivalent model of shaft system.

The coupling is treated as a torsional spring, with its rotational inertia distributed between the motor shaft and the lead screw shaft. The lead screw mechanism operates on the principle of screw transmission, where the ball screw transmits force and motion through the contact of balls, involving Hertzian contact stiffness. Considering the coupling of geometric errors, and for convenience of description, the nut along with the load is collectively referred to as the nut. For the nut alone, its equivalent motion model is expressed as Figure 4:

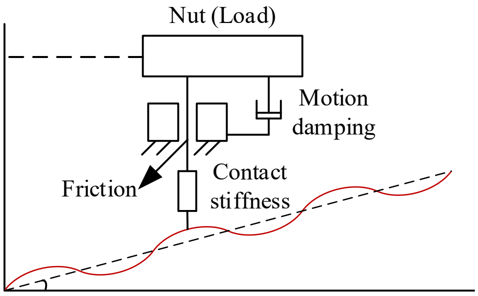

Figure 4: Equivalent model of nut coupling geometric error.

In the figure above, the contact stiffness is provided by the balls, while the resistance of the nut and load is determined by the guideway, including damping and friction. The vertical direction represents the displacement of the nut. The balls contribute to the contact stiffness, and the vertical length in the equivalent model of the nut is merely illustrative and is not included in the specific calculation process. By combining the above models, the dynamic equations of the system can be derived. For the motor subsystem:

$$\begin{cases} L\dfrac{di_a}{dt}+Ri_a=u_a+K_e\omega_m\sin(p\theta_m) \\ L\dfrac{di_b}{dt}+Ri_b=u_b-K_e\omega_m\cos(p\theta_m) \\ T_{em}=-K_t(i_a\sin(p\theta_m)-i_b\cos(p\theta_m)) \\ J_{m-eq}\dfrac{d^2\theta_m}{dt^2}+(B_m+B_c)\dfrac{d\theta_m}{dt}-B_c\dfrac{d\theta_s}{dt}+\theta_m=T_{em}+k_c\theta_s \end{cases} \tag{1}$$

In the above equation, u_a and u_b represent the phase voltages of phases A and B, respectively; i_a and i_b represent the phase currents of phases A and B, respectively; R is the phase resistance; L is the phase inductance; K_e and K_t are the back electromotive force constant and torque constant, respectively; J_{m-eq} is the equivalent moment of inertia of the motor shaft; θ_m and θ_s are the angular displacements of the motor shaft and lead screw shaft, respectively; ω_m and B_m are the angular velocity and damping coefficient of the motor shaft, respectively; p is the number of rotor teeth; k_c and B_c are the torsional stiffness and torsional damping of the coupling, respectively. As motion is transmitted to the lead screw shaft, the following equation holds:

$$\begin{cases} \dfrac{d\theta_s}{dt}=\omega_s \\ \dfrac{d\omega_s}{dt}=\dfrac{1}{J_{s-eq}}[k_c(\theta_m-\theta_s)+B_c(\theta_m-\theta_s)+ \\ k_nh(l+\dfrac{de}{d\theta_s})-B_s\omega_s-T_{fs}] \end{cases} \tag{2}$$

In the above equation, ω_s represents the angular velocity of the lead screw shaft; J_{s-eq} denotes the equivalent moment of inertia of the lead screw shaft; k_n and B_s are the contact stiffness and damping, respectively; l is the lead of the screw; e stands for geometric errors; h is the deformation of the contact spring; and T_{fs} represents the nonlinear friction resistance. The nut and load can be described by the following equation:

$$\begin{cases} \dfrac{dx_T}{dt}=v_T \\ \dfrac{dx_T}{dt}=\dfrac{1}{m_T}[-k_nh-b_nv_T-f_n] \end{cases} \tag{3}$$

In the above equations, x_T, v_T and m_T denote the displacement, velocity, and mass of the nut, respectively; b_n is the translational damping coefficient of the nut; and f_n represents the nonlinear translational damping of the nut, which is quantitatively expressed using the Stribeck friction model. The intermediate variables in Equations (1), (2), and (3) are defined as follows:

$$\begin{cases} x_i = l\theta_s \\ e = C\sin(\dfrac{2\pi x_i}{T} + \varphi) \\ h = x_T - x_i - e \end{cases} \tag{4}$$

In the above equation, x_i is the ideal displacement; C, T and φ represent the amplitude, period, and selected initial phase of the geometric error, respectively. The Stribeck friction model for the rotational friction of the lead screw and the translational friction of the nut is expressed as follows:

$$\begin{cases} T_{fs} = T_{cs} + (T_{ss} - T_{cs})\exp\left(-\left(\dfrac{|\omega_s|}{\omega_{ss}}\right)^{\delta s}\right) \\ f_n = f_{cn} + (f_{sn} - f_{cn})\exp\left(-\left(\dfrac{|v_T|}{v_{sn}}\right)^{\delta n}\right) \end{cases} \tag{5}$$

In the above equations, T_{cs} is the coulomb friction torque of the lead screw rotation, T_{ss} is the static friction torque, ω_{ss} is the characteristic angular velocity, and δ_s is the exponential coefficient for the lead screw angular velocity; f_{cn} is the coulomb friction force of the nut translation, f_{sn} is the static friction force, v_{sn} is the characteristic velocity, and δ_n is the exponential coefficient for the nut velocity. The system of equations integrates the driving mode of the stepper motor, relying solely on pulse frequency and pulse count for motion transmission and conversion.

3. Micro-Stroke Motion Characteristics Simulation

According to the Oriental Motor Product Manual[12], Table 1 lists the dynamic parameters of the PKP223D15-series stepper motor. Based on reference to the mechanical structure, material properties, and related analysis of the same type of ball screw used in the precision linear platform, the corresponding physical parameters are presented in Table 2.

Table 1: Dynamic parameters of the stepper motor.

Physical parameters	Unit	Value
Maximum excitation torque	N·m	0.095
Rated current per phase	A	1.5
Winding resistance per phase	Ω	1.18
Winding inductance per phase	mH	0.96
number of totor teeth	—	50
moment of inertia of motor Shaft	kg·m^2	10^{-6}
rated boltage per phase	V	1.77
rotor viscous damping	N·m·s/rad	10^{-5}

Table 2: Dynamic parameters of the precision linear platform.

Physical parameters	Unit	Value
Moment of Inertia of Coupling	kg·m^2	3×10^{-7}
Torsional Stiffness of Coupling	N·m/rad	44
Torsional Damping of Coupling	N·m·s/rad	10^{-6}
Moment of Inertia of Lead Screw Shaft	kg·m^2	3.36×10^{-7}
Rotational Damping of Lead Screw Shaft	N·m·s/rad	10^{-5}
Lead	mm/rev	1
Mass of Nut and Load	kg	0.2
Contact Stiffness of Balls	N/m	1.5×10^4

The δ exponent adopts the commonly used empirical value δ=2[13]. The corresponding parameters of the Stribeck friction model are presented in Table 3.

Table 3: Dynamic parameters of the precision linear platform.

Physical parameters	Unit	Value
Moment of Inertia of Coupling	$kg \cdot m^2$	3×10^{-7}
Torsional Stiffness of Coupling	$N \cdot m/rad$	44
Torsional Damping of Coupling	$N \cdot m \cdot s/rad$	10^{-6}
Moment of Inertia of Lead Screw Shaft	$kg \cdot m^2$	3.36×10^{-7}
Rotational Damping of Lead Screw Shaft	$N \cdot m \cdot s/rad$	10^{-5}
Lead	mm/rev	1
Mass of Nut and Load	kg	0.2
Contact Stiffness of Balls	N/m	1.5×10^{4}

Substituting the parameters from Tables 1, 2, and 3 into the differential equations, dynamic simulation was performed using MATLAB. Focusing on the motion characteristics at micro-strokes and emphasizing velocity—one of the three fundamental elements of motion—simulation was carried out for strokes of 10 μm and 20 μm at a frequency of 200 Hz. See Figure 5 for the corresponding velocity-time plots for the 10 μm and 20 μm stroke scales.

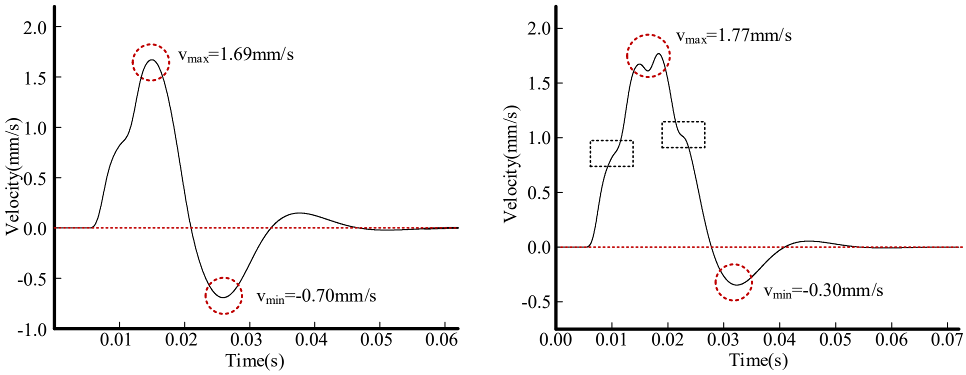

(a) Velocity-time simulation for 10 μm stroke. *(b) Velocity-time simulation for 20 μm stroke.*

Figure 5: Velocity-time simulation for 10 μm stroke and 20 μm stroke.

For larger strokes, simulations were performed for 50 μm and 100 μm. The velocity-time plots reflecting the motion characteristics are shown in Figure 6.

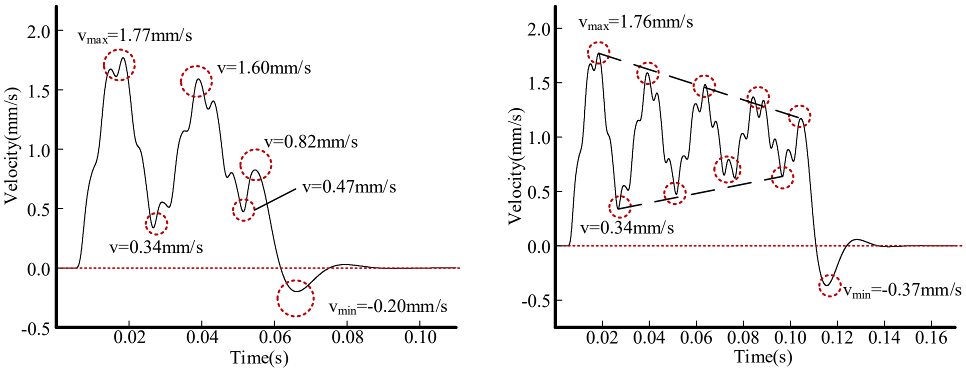

(a) Velocity-time simulation for 50 μm stroke. *(b) Velocity-time simulation for 100 μm stroke.*

Figure 6: Velocity-time simulation for 50 μm stroke and 100 μm stroke.

Observing Figures 5 and 6, the following results can be preliminarily obtained: (1) Velocity exhibits aperiodic fluctuations, with instances of reversals in velocity; (2) The response of the previous step has not yet fully settled before the next step begins, leading to overlapping effects and consequently multiple local peaks and troughs; (3) Due to the presence of electrical damping, the braking efficiency is relatively high, enabling the system to quickly reach a steady state.

4. Comparison between simulation and experiment

The experimental setup for measuring the motion characteristics of the precision motion platform is shown in Figure 7. The experiment was conducted under constant temperature and humidity conditions with minimal interference. A Renishaw XL-80 laser interferometer (Renishaw, UK) was used, with a system accuracy of ±0.5 ppm (0–40 °C), a resolution of 0.001 µm, a maximum measurement speed of 4.0 m/s, and a maximum sampling frequency of 50 kHz. The precision linear platform under test has a deadweight of 0.78 kg, a unidirectional positioning accuracy within 5 µm, a repeatability within 0.5 µm, and a maximum operating speed of 20 m/s.

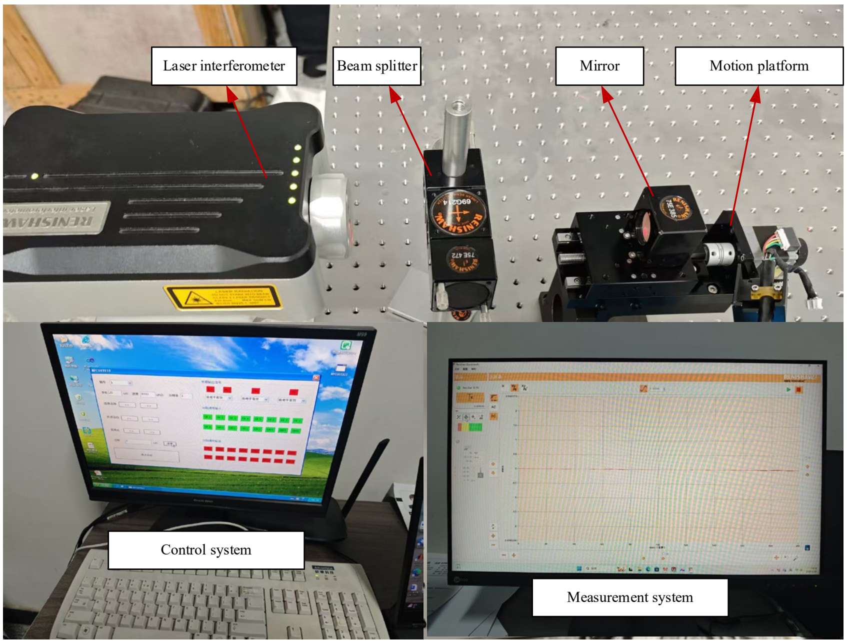

Figure 7: Experimental Setup for Motion Characteristics Measurement.

The mirror is not fixedly connected to the worktable; its constraint is provided solely by the contact force at the interface. Therefore, a slight tapping experiment was conducted to measure the natural decay oscillation process between the beam splitter and the worktable. The corresponding experimental principle is shown in Figure 8. The first trough after excitation was ensured to exceed 0.5 mm/s to match the first trough in the simulation. Sampling was performed at intervals of 0.1 ms. The measured velocity-time plot is shown in Figure 9.

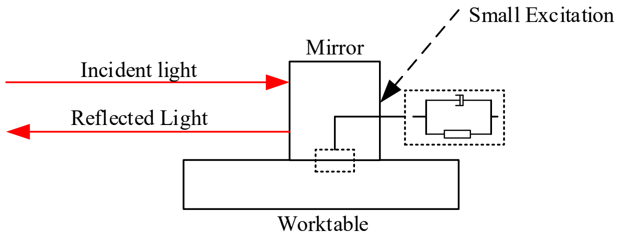

Figure 8: Measurement principle of mirror decay oscillation.

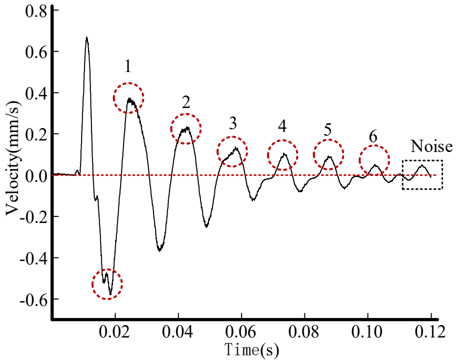

Figure 9: Natural decay oscillation process of the mirror.

It can be observed from the figure that, starting from the first trough, the decay oscillation process dominated by contact damping exhibits six peaks before the remaining portion can be considered as noise. Therefore, in the subsequent experimental measurement curves, the portion after the first trough is neglected to correspond with the simulation results.

Sampling measurements were performed at intervals of 0.1 ms, and experimental comparisons were conducted following the step size and frequency used in the simulation. First, motion characteristic measurement experiments were carried out for micro-strokes of 10 μm and 20 μm. The resulting velocity-time plots are shown in Figure 10.

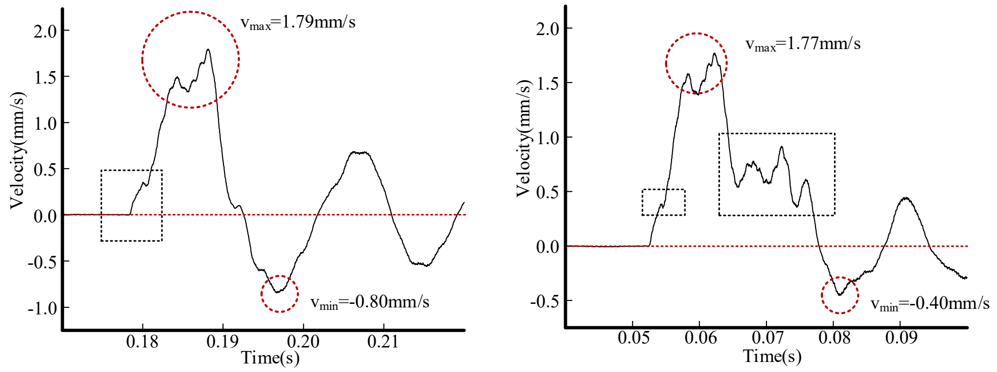

(a) Velocity-time simulation for 10 μm stroke. (b) Velocity-time simulation for 20 μm stroke.

Figure 10: Velocity-time measurement curves for 10 μm and 20 μm strokes.

Comparing the simulation results with the experimental measurements, at the 10 μm stroke scale, the simulated maximum velocity is 1.69 mm/s, while the corresponding measured velocity is 1.79 mm/s; the simulated minimum velocity is −0.7 mm/s, and the corresponding measured velocity is −0.8 mm/s. From the waveform comparison, the simulation demonstrates a certain predictive capability regarding velocity fluctuations during operation. At the 20 μm stroke scale, the simulated maximum velocity is 1.77 mm/s, matching the measured value of 1.77 mm/s; the simulated minimum velocity is −0.3 mm/s, while the measured minimum is −0.4 mm/s. In terms of waveform comparison, the simulation captures the double peaks, with the second peak appearing higher than the first, and also predicts velocity fluctuations at approximately the corresponding waveform positions. Compared with conventional equivalent models, the proposed model achieves a higher degree of predictive accuracy for velocity variations. Then, motion characteristic measurement experiments were conducted for strokes of 50 μm and 100 μm. The resulting velocity-time plots are shown in Figure 11.

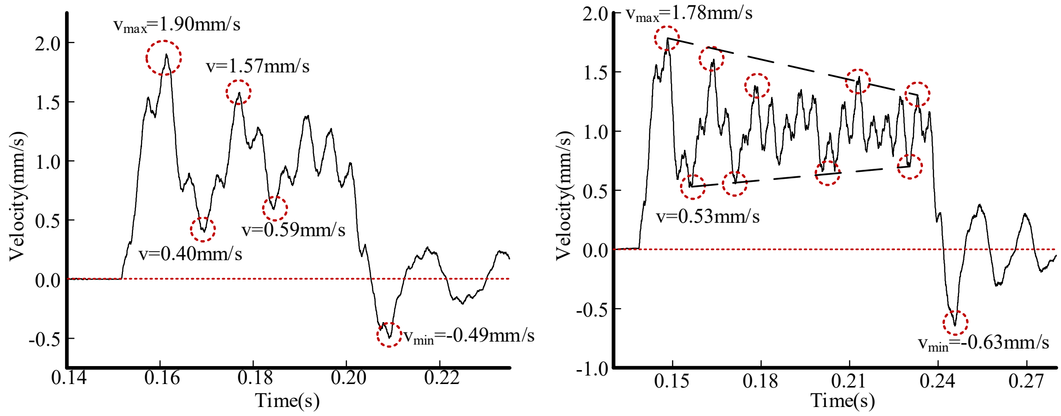

(a) Velocity-time simulation for 50 μm stroke. (b) Velocity-time simulation for 100 μm stroke.

Figure 11: Velocity-time measurement curves for 10 μm and 20 μm strokes.

Comparing the similarities between the simulation and experiment at the 50 μm stroke, the measured curve first exhibits successive local peaks, which is similar to the simulation, followed by local troughs, then rises to local peaks again, and subsequently decreases to local troughs. If the final fluctuations are considered as a set of local peaks, the alternating sequence of peaks and troughs is consistent with the simulation. The greatest discrepancy in velocity occurs at the maximum overshoot velocity after the pulse stops.

Due to the large number of local peaks and troughs, the comparison between simulation and experiment at the 100 μm stroke focuses primarily on the overall trend. It can be observed from the figure that both the simulation and experimental results converge toward a velocity of 1 mm/s, which corresponds to the average velocity at a frequency of 200 Hz. The simulated curve exhibits a total of five sets of local peaks and four sets of local troughs, while the experimental curve can be interpreted as having five local peaks and four local troughs. The greatest velocity discrepancy is again observed at the maximum overshoot velocity after the pulse stops.

To compare the proposed refined model with a conventional equivalent model, a simplified second-order equivalent dynamic model of the ball screw system was established. In this simplified model, the motor was driven with a gradually decreasing torque under open-loop conditions, and linear friction was incorporated. Velocity-time plots were simulated for displacements of 10 μm, 20 μm, 50 μm, and 100 μm, as shown in Figure 12.

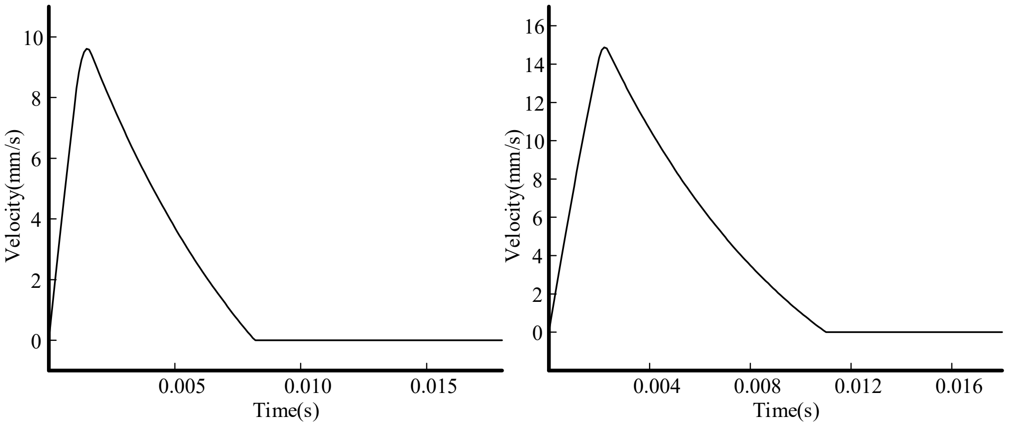

(a) Velocity-time simulation for 10 μm stroke. (b) Velocity-time simulation for 20 μm stroke.

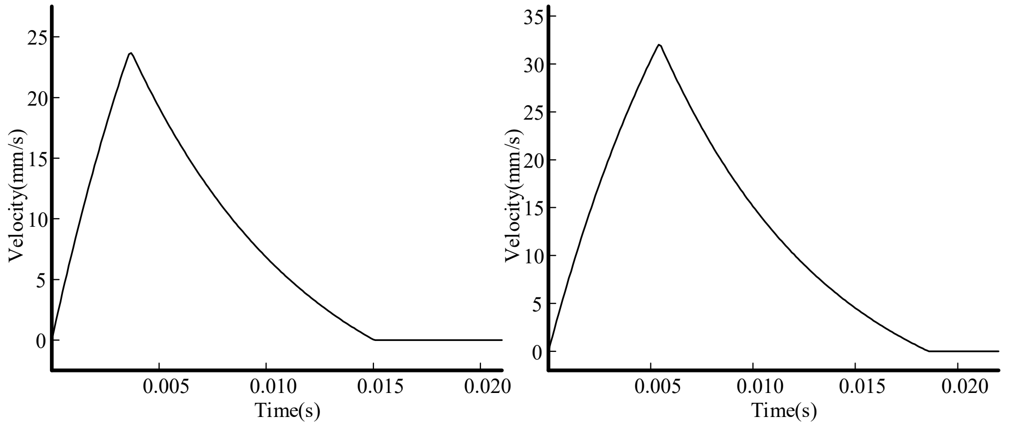

(c) Velocity-time simulation for 50 μm stroke. (d) Velocity-time simulation for 100 μm stroke.

Figure 12 : Velocity-time plots for various strokes using conventional second-order equivalent model.

It can be observed that due to the extremely small stroke, the system cannot reach a state of equilibrium where the input force equals the resistance. Consequently, the velocity does not converge, nor does it exhibit the oscillatory behavior with multiple local peaks and troughs seen in actual motion. Moreover, under open-loop conditions, the velocity increases significantly.

5. Conclusion

It can be observed that due to the extremely small stroke, the system cannot reach a state of equilibrium where the input force equals the resistance. Consequently, the velocity does not converge, nor does it exhibit the oscillatory behavior with multiple local peaks and troughs seen in actual motion. Moreover, under open-loop conditions, the velocity increases significantly.

(1) By introducing equivalent component models that account for the stepper motor and lead screw errors, the dynamic model of this type of precision linear motion platform is refined. Compared with conventional second-order equivalent dynamic models, the proposed model better captures the motion characteristics at micro-stroke scales under actual operating conditions and enables a certain degree of

prediction of velocity fluctuations and velocity magnitude during motion.

(2) The refined dynamic model developed following the approach presented in this study provides theoretical support for further in-depth investigation of the other two fundamental motion elements—displacement and acceleration—in future research.

(3) Regarding the limitations of the proposed model, for macro-stroke and high-speed operating conditions, future work may incorporate additional nonlinear factors such as the torque–speed characteristics of the stepper motor and pulse accuracy. Furthermore, increasing the complexity of the coupling mechanism between geometric errors in the ball screw system will further approximate the actual operating process.

References

[1] AGUADO S, PEREZ P, ALBAJEZ J A. Study on Machine Tool Positioning Uncertainty Due to Volumetric Verification[J]. Sensors (Basel), 2019, 19(13) :2847.

[2] Z C Du, J Wu, J G Yang. GeometricError Modeling and Sensitivity Analysis of Single-Axis Assembly in Three-Axis Vertical Machine Center Based on Jacobian-Torsor Model[J]. ASCE-ASME J Risk and Uncert in Engrg Sys Part B Mech Engrg, 2017, 4(3): 48-62.

[3] Y B Huang, K C Fan, Z F Lou, et al. A novel modeling of volumetric errors of three-axismachine tools based on Abbe and Bryan principles[J]. International Journal of Machine Tools and Manufacture, 2020:151.

[4] R R Qian, M Z Luo, J H Zhao, et al. Modeling and Dynamic Research Based on Ritz Series for Ball Screw Drive System[J].Journal of System Simulation, 2017,29(10):2268-2275.

[5] J Wu, M Y Li, P B Zhang, et al. Modeling and Analysis of Motion Error of Ram Type Hydrostatic Guide[J/OL]. Modular Machine Tool and Automatic Manufacturing Technique,2026.

[6] H Tang, H Zhang, D Zhang, et al. Repeatability Characterization and Compensation in Micro-scale Displacement for Precise Linear Stage Based on Micro-dynamics Analysis[J].Journal of Mechanical Engieering, 2023,59(21):110-120.

[7] T Huang, S J Du, Q Zhang, et al. Experimental Modeling of Linear Parameter Varying Dynamics Model of Ball Screw Drive System[J]. Journal of Mechanical Engineering, 2022,58(9):98-106.

[8] J J Zhao, M X Lin, X C Song, et al. Modeling and Analysis of Full Ball Load Distribution of Ball Screw with the Combined Load[J]. Journal of Mechanical Engineering, 2020, 56(17):126-136.

[9] J Cha,H J Zhang. Modeling on Motion Error of Vertical Hydrostatic Cylindrical Guideways[J]. Journal of Mechanical Engineering, 2023,59(09):116-124.

[10] H Ohta, K Tanaka. Vertical stiffness of preloaded linear guideway type ball bearing incorporating the flexibility of the carriage and rail[J]. Journal of Tribology-Transactions of the ASME, 2010, 132(1):1-9.

[11] G Khim,J S Oh,C H Park. Analysis of 5-DOF motion errors influenced by the guide rails of an aerostatic linear motion stage[J]. International Journal of Precision Engineering and Manufacturing, 2014, 15(2):283-290.

[12] Oriental Motor. Stepper Motor PKP Series [EB/OL]. https://www.orientalmotor.com.cn/products/stepping-motors/2-phase-pkp-pk.

[13] T Zhang, J H He, Y P Shi, et al. Dynamic Parameter Identification of Collaborative Robot Based on Improved Stribeck Friction Model [J/OL]. Journal of Mechanical Engineering, 2026.